Optomagnonics in magnetic solids

Tianyu Liu, Xufeng Zhang, Hong X. Tang, and Michael E. Flatté

Phys. Rev. B **94**, 060405 — Published 9 August 2016

DOI: 10.1103/PhysRevB.94.060405

Optomagnonics in Magnetic Solids

Tianyu Liu,[1] Xufeng Zhang,[2] Hong X. Tang,[2] and Michael E. Flatté[1]

[1] *Optical Science and Technology Center and Department of Physics and Astronomy, University of Iowa, Iowa City, Iowa 52242, USA*

[2] *Department of Electrical Engineering, Yale University, New Haven, CT 06520, USA*

Coherent conversion of photons to magnons, and back, provides a natural mechanism for rapid control of interactions between stationary spins with long coherence times and high-speed photons. Despite the large frequency difference between optical photons and magnons, coherent conversion can be achieved through a three-particle interaction between one magnon and two photons whose frequency difference is resonant with the magnon frequency, as in optomechanics with two photons and a phonon. The large spin density of a transparent ferromagnetic insulator (such as the ferrite yttrium iron garnet) in an optical cavity provides an intrinsic photon-magnon coupling strength that we calculate to exceed reported optomechanical couplings. A large cavity photon number and properly selected cavity detuning produce a predicted effective coupling strength sufficient for observing electromagnetically induced transparency and the Purcell effect, and even to reach the ultra-strong coupling regime.

Cavity optomechanics, the optical control of mechanical excitations, has formed the framework for demonstrations of slow light [1] and squeezed light [2], and proposals for quantum memory [3]. In cavity optomechanics, radiation pressure couples the photons in optical or microwave cavities to the phonons of mechanical resonators. In addition to clarifying the fundamental nature of quantum interactions and noise, such studies can be applied to systems in which each excitation provides advantages; *e.g.* in quantum memory the photons serve as broad-band long distance information carriers and the phonons as long-time information storage. Spin waves, like elastic waves, are collective excitations and interact with light. Spin waves, however, are more easily decoupled from the environment than elastic waves, and can also be efficiently manipulated magnetically (in addition to electrically). These advantages suggest a new field, spin optodynamics, or "optomagnonics", in which optical or microwave fields are paired with these collective spin excitations, whose quanta are known as magnons. Magnons have been shown to efficiently replace radiofrequency (RF) phonons in microwave cavities, in which strong and ultra-strong couplings of magnons and microwave photons have been achieved via the interaction between magnons and the oscillating magnetic fields of the microwave photons [4–8]. Recent realizations of weak optical whispering gallery mode coupling to magnetostatic spin waves in a yttrium iron garnet (YIG) sphere are perhaps the first examples of cavity optomagnonics [9–12].

Here we describe a theoretical framework for optomagnonics, which takes place through the magnon-photon interaction in an optical cavity containing a magnetic slab as shown in Fig. 1. As in cavity optomechanics [13–16], in which the presence of elastic waves modifies the light transmission, here light transmission is modified by the magnetic media and the presence of magnons. In a microwave cavity a magnon couples to the magnetic component of the RF fields, and a microwave photon converts directly into a magnon, or vice versa, through a two-particle interaction. For the optomagnonic configuration a three-particle interaction couples a magnon and the electric component of the optical fields within the optical cavity. From the electron-radiation interaction, we calculate the intrinsic magnon-photon coupling strength (g_0) in YIG and find that it can be made comparable to or larger than the intrinsic phonon-photon coupling strength in cavity optomechanics. By virtue of detuning and a large photon number, g_0 can be enhanced to reach the strong coupling regime where an effective coupling $g^{\rm eff}$ exceeds either the cavity linewidth or the magnon linewidth, and in these regimes electromagnetically induced transparency [1, 5, 17] and a Purcell enhancement [5, 18–20] can be achieved. We find even the ultra-strong regime in which $g^{\rm eff}$ exceeds both is feasible. These developments in optomagnonics may also assist the low-dissipation propagation of magnons in spintronic devices. For example, an optomagnonic arrangement may form the basis for a high-efficiency, low-dissipation hybrid spintronic interconnect that transmits spin information in optical form. Developments in understanding coherent conversion between magnons and photons may therefore assist in connecting spintronic devices to a network for quantum communication. Furthermore, the nonreciprocal nature of the magnetic system allows for an isolating, diode-like character of the switching from one mode to another; that is, a first mode can be switched into a second, whereas the second mode does not switch into the first.

Intrinsic photon-magnon interactions.—Photons interact with magnons through linear and quadratic magneto-optical coupling,

$$H_I = \frac{1}{8}\int dV \epsilon_0 \left\langle \sum_{\alpha,\beta} \epsilon_r^{\alpha\beta}(\mathbf{M}) E_1^{\alpha *} E_2^{\beta} + h.c. \right\rangle_{time}, \quad (1)$$

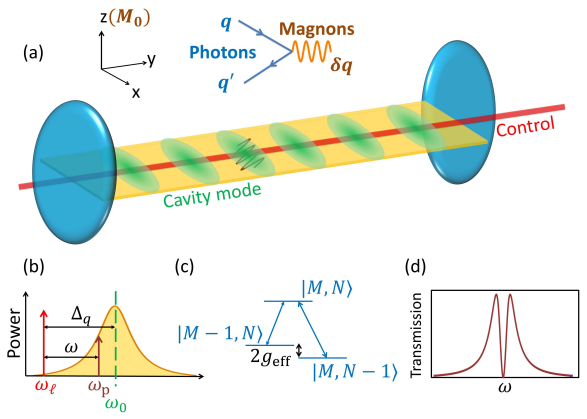

Figure 1. (a) Schematic illustration of cavity optomagnonics. The yellow slab sandwiched by two mirrors is the cavity for magnons and for optical photons. (b) ω_ℓ, $\omega_{\rm p}$ and ω_0 denote the frequencies of the control light, the probe light, and the optical cavity mode, respectively. The yellow wave package shows the linewidth of the probe light. (c) $g^{\rm eff}$ splits two polariton states with different control light and probe light photon number. (d) Due to the three-particle interaction between magnons and photons, the transmission spectra can be tuned by the control light produce a transparency window around the frequency of magnon modes.

where $\epsilon_r^{\alpha\beta}(\mathbf{M})$ $(\alpha,\beta = x,y,z)$ is the relative dielectric tensor as a function of the magnetization (which includes the effect of magnons). The time average ensures energy conservation. The subscripts "1" and "2" denote two light beams that interact with the magnetization,

$$E_i^\alpha = iE_{0i}\sum_{q_i,m} e_{i,m}^\alpha(\xi,\zeta)a_{i,m}^\dagger e^{-iq_i\eta+i\omega_i t}\,, \tag{2}$$

where $i=1,2$, $E_{0i}=(2\hbar\omega_i/\epsilon_0 n_0^2 V)^{1/2}$ (with n_0 being the refractive index of YIG) and η, ξ and ζ are the coordinates along the length, width and thickness respectively. We consider $\omega_1\approx\omega_2=(2\pi c_0)/(n_0\lambda_0)$ with c_0 the speed of light in vacuum, as the excited magnons have much less energy than the photons. $e_{i,m}^\alpha(\xi,\zeta)$ are the normalized field functions for different optical cavity modes, and $a_{i,m}^\dagger$ is the creation operator for cavity mode m. Here m is a simplified notation for different modes, including distinguishing transverse electric (TE) and magnetic (TM). Although each field is written as a propagating wave, the summation with its hermitian conjugate yields the appropriate cavity standing wave. YIG is almost transparent, so we consider only the hermitian part of the dielectric tensor. For crystals with cubic symmetry and assuming the saturation magnetization is along the [001] direction, we have, up to linear order in M_x and M_y,

$$\epsilon_r(\mathbf{M}) = \begin{pmatrix} 0 & 0 & \epsilon_r^{xz} \\ 0 & 0 & \epsilon_r^{yz} \\ \epsilon_r^{zx} & \epsilon_r^{zy} & 0 \end{pmatrix}\,, \tag{3}$$

with $\epsilon_r^{xz} = -iKM_y + 2G_{44}M_xM_0$, $\epsilon_r^{yz} = iKM_x + 2G_{44}M_yM_0$, $\epsilon_r^{zx} = (\epsilon_r^{xz})^*$ and $\epsilon_r^{zy} = (\epsilon_r^{yz})^*$, where $\mathbf{M}_0 \parallel \hat{z}$ is the saturation magnetization [21, 22]. K and G_{44} can be obtained from measurements [21, 22] of the magnetic circular birefringence,

$$\Phi_{\rm MCB} = \frac{\pi M_0 K}{\lambda_0 n_0} \quad \text{for } \mathbf{k}\parallel\mathbf{M}_0\,, \tag{4}$$

and the magnetic linear birefringence,

$$\Phi_{\rm MLB} = \frac{2\pi M_0^2 G_{44}}{\lambda_0 n_0} \quad \text{for } \mathbf{M}_0\parallel[111]\perp\mathbf{k}\,, \tag{5}$$

with λ_0 the wavelength of the incident light. Applying the Holstein-Primakoff transformation [23] to the magnetization we find

$$M^+(\mathbf{r}) = \left(\frac{2\hbar\gamma M_0}{V}\right)^{\frac{1}{2}}\sum_{n,k} b_k e^{ik\eta}\phi_n(\xi,\zeta)\,, \tag{6}$$

$$M^-(\mathbf{r}) = \left(\frac{2\hbar\gamma M_0}{V}\right)^{\frac{1}{2}}\sum_{n,k} b_k^\dagger e^{-ik\eta}\phi_n(\xi,\zeta)\,, \tag{7}$$

where γ is the gyromagnetic ratio and $\phi_n(\xi,\zeta)$ are the normalized functions for different magnon modes. We assume the cavity is subject to pinned magnetic boundary conditions on the edges of its cross section, that is

$$\phi_n(\xi,\zeta) = \cos\left(\frac{n\pi\xi}{2w}\right)\,, \tag{8}$$

where $n=1,3,5,...$ and w is the half width of the cavity. As the magnon modes we consider have frequencies of several GHz, and the dimension along the thickness direction is small comparing with the magnon wavelength, we regard the magnon wave function as homogeneous along the direction of the slab thickness and so independent of ζ. The photon-magnon interaction then simplifies to

$$\begin{aligned} H_I = \sum_{m,m',k_n}\Big[&\hbar g_{mm'n}^{(+)} a_m a_{m'}^\dagger b_{k_n}\delta(q_m - q_{m'} + k_n) \\ &+\hbar g_{mm'n}^{(-)} a_m a_{m'}^\dagger b_{k_n}^\dagger\delta(q_m - q_{m'} - k_n)\Big]\,, \end{aligned} \tag{9}$$

with

$$\begin{aligned} g_{mm'n}^{(\pm)} = &\left(\frac{2\hbar\gamma}{M_0 V}\right)^{\frac{1}{2}}\frac{c_0}{n_0^2} \\ &\times[\Phi_{\rm MLB}G_{44,mm'n}^{(\pm)} \pm \Phi_{\rm MCB}K_{mm'n}^{(\pm)}]\,, \end{aligned} \tag{10}$$

where

$$\begin{aligned} G_{44,mm'n}^{(\pm)} = \frac{1}{S}\int_{-w}^{w}d\xi\int_{-d}^{d}d\zeta\,\big(&e_{1m,z}^* e_{2m',x} \mp ie_{1m,z}^* e_{2m',y} \\ &+e_{1m,x}^* e_{2m',z} \mp ie_{1m,y}^* e_{2m',z}\big)\,\phi_n(\xi,\zeta) \end{aligned} \tag{11}$$

$$\begin{aligned} K_{mm'n}^{(\pm)} = \frac{1}{S}\int_{-w}^{w}d\xi\int_{-d}^{d}d\zeta\,\big(&e_{1m,z}^* e_{2m',x} \mp ie_{1m,z}^* e_{2m',y} \\ &-e_{1m,x}^* e_{2m',z} \pm ie_{1m,y}^* e_{2m',z}\big)\,\phi_n(\xi,\zeta)\,, \end{aligned} \tag{12}$$

and $S=4wd$ is the area of the cavity cross section. The anti-Stokes and Stokes processes have different coupling

rates $g^{(\pm)}_{mm'n}$, and $g^{(+)}_{mm'n} = g^{(-)*}_{m'mn}$ due to $G^{(\pm)*}_{44,mm'n} = G^{(\mp)}_{44,m'mn}$ and $K^{(\pm)*}_{mm'n} = -K^{(\mp)}_{m'mn}$. This asymmetry has recently been observed in the coupling between whispering gallery modes and magnon modes [11]. Here, we have explicitly written down the dependence of the intrinsic coupling rate $g^{(\pm)}_{mm'n}$ on cavity and magnon mode numbers. For given mode numbers, we will use $g^{(\pm)}_0$ for simplicity instead of $g^{(\pm)}_{mm'n}$. $\Phi_{\rm MCB} \approx \Phi_{\rm MLB} = 6.1$ rad/cm for YIG [22, 24], so we obtain $g^{(-)}_0 \approx 2\pi \times 27$ Hz for the Stokes process (TE$_{00}\rightarrow$TM$_{31} + \phi_3$ with ϕ_3 the $n = 3$ magnon mode) of 1.55-μm incident light. A selection rule restricts transitions to those between different polarizations if $\Phi_{\rm MCB} = \Phi_{\rm MLB}$. Changing the ratio of $\Phi_{\rm MCB}$ to $\Phi_{\rm MLB}$ allows TE to TE and TM to TM transitions but the resulting rates are still much smaller than the TE to TM transitions. The nonreciprocal behavior of transition from one mode to another is unique to the optomagnonic system, for time-reversal symmetry is broken. In the strong coupling regime discussed later, this feature and electromagnetically induced transparency produces an optical diode, in which probe light of the TE mode is totally reflected into the TM mode, but is absorbed by the cavity for the other modes (including TM to TE). The nature of the control light interaction allows the direction of this optical diode to be switched with the frequency of the control light: red detuning allows TM→TE but prevents TE→TM, whereas blue detuning allows TE→TM but prevents TM→TE.

The coupling rate also depends on the mode numbers. Along the thickness direction, the lowest two optical modes together with the homogeneous magnon mode yield the largest modal overlap. For the width direction, the coupling rates of the opposite-parity TE to TM transitions of other mode numbers differ from that value by less than 1%. The parity requirement ensures the integrand in Eqs. (11) and (12) is an even function along the width of the cavity.

The intrinsic photon-magnon coupling strengths in YIG exceed the reported photon-phonon coupling strength ($2\pi \times 2.7$ Hz) in a cavity that supports strong optomechanical coupling [13], suggesting the potential for cavity optomagnonics. Comparing the interaction Hamiltonian in the electro-optical, optomechanical and optomagnonic systems using the same effective Hamiltonian, $H_I = (\hbar\varphi/\tau)a^\dagger a(b + b^\dagger)$, with φ (τ) the optical phase shift (time) of a single round trip, the interaction strength and quality factor Q_m for the three systems are reported in Table I with uniform parameters where possible and typical values for the electro-optical and optomechanical systems [25]. Table I shows that, within the same optical cavity, the optomagnonic coupling is ten times larger than the optomechanical coupling, as is the corresponding quality factor. Although the electro-optical coupling is even stronger, the poor quality factor of the fundamental frequency makes strong coupling in an electro-optical system much more difficult than in the other two systems.

Table I. Comparison of the coupling rates in electro-optical [26], optomechanical [13] and optomagnonic systems.

	Electro-optical	Optomechanical	Optomagnonic
$\frac{\varphi}{\omega_0\tau}$	$\frac{n_0^2 r}{2d}\sqrt{\frac{\hbar\omega_m}{2C}}$	$\frac{1}{l}\sqrt{\frac{\hbar}{2m\omega_m}}$	$\frac{K}{2n_0^2}\sqrt{\frac{\hbar\gamma M_0}{V}}$
values	1.2×10^{-11}	3.1×10^{-14}	3.1×10^{-13}
Q_m	500	10^4	10^5

Spin optodynamics in cold atoms (^{87}Rb with D_2 transition) [27–29] has been proposed, so we also compare the cold atom g_0 following our three-particle definition (differing from the convention in Ref. [27]) to YIG. The linear magneto-optical coupling in the dielectric tensor ($K\epsilon_{\alpha\beta\tau}M_\tau$, where $\epsilon_{\alpha\beta\tau}$ is the Levi-Civita tensor) has the same form for both YIG and the vector AC-Stark effect in cold atoms. For cold atoms $K = (d^2 v)/(\epsilon_0\hbar^2\Delta_{ca}\gamma)$ for ^{87}Rb with d the electric dipole of the D_2 transition [30], v the vector shift, ϵ_0 the vacuum permittivity, Δ_{ca} the detuning between the cavity resonance and the D_2 transition frequency, and γ the gyromagnetic ratio. Although $K(^{87}\text{Rb})/K(\text{YIG}) \sim 10^7$, the spin density ratio is so small that $M_0(^{87}\text{Rb})/M_0(\text{YIG}) \sim 10^{-11}$. As $g_0 \propto K\sqrt{M_0}$, $g_0(^{87}\text{Rb})$ is of similar order as g_0(YIG).

Strong coupling regimes—-In analogy to cavity optomechanics, we consider control light acting on the cavity as shown in Fig. 1(a) to enhance the photon-magnon interaction by a factor of $\sqrt{N_\ell}$ (with N_ℓ the number of control light photons with frequency ω_ℓ). This can be understood in a frame rotating with ω_ℓ, where q denotes the cavity resonance mode. Considering the cavity modes q and q' with specific transverse mode numbers m and m', we will drop the subscripts of m and m' for simplicity. The system is then described by

$$\begin{aligned} H = &\sum_q \hbar\Delta_q a_q^\dagger a_q + \sum_{n,k} \hbar\omega_{nk} b_k^\dagger b_k \\ &+ \sum_{n,q,q',k} \Big[\hbar g^{(+)}_{qq'n} a_q a_{q'}^\dagger b_k \delta(q - q' + k) \\ &+ \hbar g^{(-)}_{qq'n} a_q a_{q'}^\dagger b_k^\dagger \delta(q - q' - k)\Big] , \end{aligned} \tag{13}$$

where $\Delta_q \equiv \omega_\ell - \omega_q$ is the detuning of a control light at frequency ω_ℓ from the cavity resonance frequency $\omega_q \equiv \omega_0$, and a_q (b_k) are the annihilation operators for the optical cavity modes (magnon of frequency ω_k).

We derive the equations of motion for b_k and a_q from the Heisenberg equation, and find

$$\dot{b}_k = -(i\omega_k + \frac{\gamma_m}{2})b_k - i\sum_{n,q} i g^{(-)}_{q,q-k,n} a_q a^\dagger_{q-k} , \tag{14}$$

$$\begin{aligned} \dot{a}_q = &-(i\Delta_q + \frac{\kappa_q}{2})a_q \\ &-i\sum_{n,k'} \Big[g^{(-)}_{q+k',q,n} a_{q+k'} b^\dagger_{k'} + g^{(+)}_{q-k',q,n} a_{q-k'} b_{k'}\Big] \end{aligned}$$

$$-(\kappa_{e,q}/2)^{1/2}a_{\mathrm{in},q}(t)-\kappa_q'^{1/2}a_{i,q}(t)\,, \tag{15}$$

with $\gamma_m=\omega_m/Q_m$ the magnon damping rate, $\kappa_{e,q}$ the optical damping rate for cavity mode q, κ_q' the parasitic optical damping rate into all other channels that are undetected (representing a loss of information), and κ_q the total optical damping rate of mode q ($\kappa_q=\kappa_{e,q}/2+\kappa_q'$). Sources of κ_q' include homogeneous broadening due to a large linewidth of the cavity resonance allowing a direct conversion of the control laser into the cavity resonance mode, or an inhomogeneous broadening due to the absorption by the mirrors of the cavity.

Introducing fluctuations (δa_q and δb_k) to the steady states ($\bar{a}_q$ and $\bar{b}_k$) of the optical modes ($a_q(t)=\bar{a}_q+\delta a_q(\omega)e^{-i\omega t}$) and the magnon mode ($b_k(t)=\bar{b}_k+\delta b_k(\omega)e^{-i\omega t}$), we solve the linear Heisenberg-Langevin equations for the fluctuations in the frequency space, and obtain the cavity mode spectra,

$$\delta a_q(\omega)=\frac{-(\kappa_{e,q}/2)^{1/2}\delta a_{\mathrm{in},q}(\omega)-\kappa_q'^{1/2}a_{i,q}(\omega)}{i(\Delta_q-\omega)+\kappa_q/2-\kappa^{(-)}} \tag{16}$$

and $\delta a_q^\dagger(\omega)=[\delta a_q(-\omega)]^*$. For the lower side band of the probe light ($\omega\equiv\omega_\mathrm{p}-\omega_\ell<0$ with ω_p the frequency of the probe light), $\delta a_q(\omega)$ and $\delta a_q^\dagger(\omega)$ are resonant when the the control light is red detuned ($\Delta_q=\omega$) and blue detuned ($\Delta_q=-\omega$), respectively. The input-output boundary conditions $\delta a_{\mathrm{out},q}(\omega)=\delta a_{\mathrm{in},q}(\omega)+(\kappa_{e,q}/2)^{1/2}\delta a_q(\omega)$ and $\delta a_{\mathrm{out},q}^\dagger(\omega)=\delta a_{\mathrm{in},q}^\dagger(\omega)+(\kappa_{e,q}/2)^{1/2}\delta a_q^\dagger(\omega)$ yield the reflection amplitudes

$$r_q^{(-)}(\omega)=1-\frac{\kappa_{e,q}/2}{i(\Delta_q-\omega)+\kappa_q/2-\kappa^{(-)}} \tag{17}$$

for red detuning, and

$$r_q^{(+)}(\omega)=1-\frac{\kappa_{e,q}/2}{-i(\Delta_q+\omega)+\kappa_q/2-\kappa^{(+)}} \tag{18}$$

for blue detuning, where

$$\kappa^{(-)}(\omega)=\sum_n\left[-\frac{\left|g_{q,q-k,n}^{(-)}\right|^2N_{\ell,q-k}}{i(\omega_k-\omega)+\gamma_m/2}+\frac{\left|g_{q+k,q,n}^{(-)}\right|^2N_{\ell,q+k}}{-i(\omega_k+\omega)+\gamma_m/2}\right] \tag{19}$$

and $\kappa^{(+)}(\omega)=\left[\kappa^{(-)}(-\omega)\right]^*$ with $N_{\ell,q\pm k}=|\bar{a}_{q\pm k}|^2$ the photon number of control light with frequency $\omega_{l,q\pm k}$. The imaginary (real) part of $\kappa^{(\pm)}$ yields a correction to the resonance frequency (the line width) of the cavity mode due to the photon-magnon interaction. The interaction strength is enhanced by $\sqrt{N_{\ell,q\pm k}}$ as shown in Eq. (19). Thus

$$g_{q,q-k,n}^{\mathrm{eff}}=g_{q,q-k,n}^{(-)}\sqrt{N_{\ell,q-k}}, \tag{20}$$

so even though the intrinsic coupling rate $g_{q,q-k,n}^{(-)}$ is inversely proportional to $\sqrt{V}$, $g_{q,q-k,n}^{\mathrm{eff}}$ is proportional to the control light power and is limited by the maximum allowable photon density.

With the control light red detuned from the cavity resonance, we plot the transmission (density plot) and reflection spectra of the anti-Stokes process as shown in Fig. 2. When $\gamma_m<g^{\mathrm{eff}}<\kappa_q$, one can obtain electromagnetically induced transparency (EIT) as shown in Figs. 2(a) and (b). The asymptotic lines on the density plot denote the resonances with the cavity and with the magnon modes, respectively. The applied magnetic field is swept to tune the magnon mode frequency. When ω_k is adjusted to be in resonance with the detuned control light, a transparency window is opened in the reflection spectra and its width is determined by g^{eff}.

The EIT properties can be determined by translating Eq. (13) to the Tavis-Cummings model for the fluctuations with the control light red detuned,

$$H=\sum_q\hbar\Delta_q\delta a_q^\dagger\delta a_q+\sum_{n,k}\hbar\omega_{nk}\delta b_k^\dagger\delta b_k+\sum_{n,q,k}\left[\hbar g_{q,q-k,n}^{\mathrm{eff}}\delta a_q\delta b_k^\dagger+h.c.\right], \tag{21}$$

which yields two types of polaritons formed by cavity modes dressed by magnon modes. The energy state of the system can be labeled with polariton number, $E_{M,N}=\hbar\omega_+(N+1/2)+\hbar\omega_-(M+1/2)$ with $\omega_\pm=(1/2)[(\Delta_q+\omega_k)\pm\sqrt{(\Delta_q-\omega_k)+4|g_{q,q-k,n}^{\mathrm{eff}}|^2}]$, whose energy level diagram is shown in Fig. 1(c). ω_ℓ is on resonance for the $|M,N-1\rangle\rightarrow|M,N\rangle$ transition whereas ω_p is detuned by ω from the $|M-1,N\rangle\rightarrow|M,N\rangle$ transition. The coexistence of the control and probe light forms a dark state that makes the probe light less absorbed.

In another regime, for $\kappa_q<g^{\mathrm{eff}}<\gamma_m$, magnons are damped so fast that there are no stable polariton states. On resonance with the magnon modes, the energy of a cavity photon is transferred to a magnon and control photon and then dissipated to the environment. The yellow curve in Fig. 2(d) shows the reflection spectrum of the probe light for the off-resonant case, and the blue one for the resonant case. The reflection is strongly reduced when the probe light, interacting with the control light, is resonant with the magnon modes.

For blue-detuned control light, the change in the reflection spectra with increasing control power is shown in Fig. 3. The monotonic decrease of the linewidth as the control light power increases [Fig. 3(d)] indicates energy is transferred from the control light to the probe light. The reflection can even exceed one when the gain compensates the energy loss due to the cavity resonance. Fig. 3(e) shows that there exists a critical power at which the reflection vanishes. Furthermore the power is limited according to Eqs. (18) and (19), above which $\kappa^{(+)}=g^{\mathrm{eff}}/(\gamma_m/2)$ cancels the cavity damping rate κ_q and the reflection diverges, leading to a self-oscillation regime. Increasing the intrinsic optical

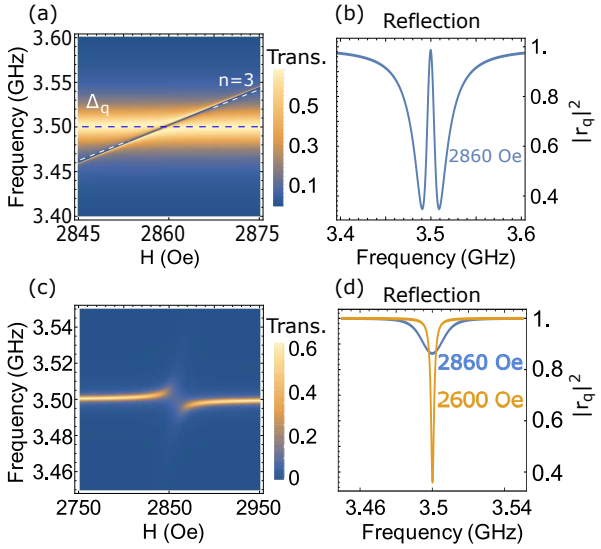

Figure 2. Transmission (density plot) and reflection spectra. (a) and (b) Electromagnetically induced transparency (EIT) with $\kappa_q = 35$ MHz, $\kappa_{e,q} = 14$ MHz, $\gamma_m = 0.1$ MHz, $g^{\rm eff} = 10$ MHz, $\Delta_q = 3.5$ GHz. (c) and (d) Purcell enhancement with $\kappa_q = 2$ MHz, $\kappa_{e,q} = 0.8$ MHz, $\gamma_m = 35$ MHz, $g^{\rm eff} = 10$ MHz, $\Delta_q = 3.5$ GHz. The frequency (ω) is the sideband shift of the probe $\omega_{\rm p}$ from the cavity resonance frequency ω_ℓ, $\omega = \omega_{\rm p} - \omega_\ell$.

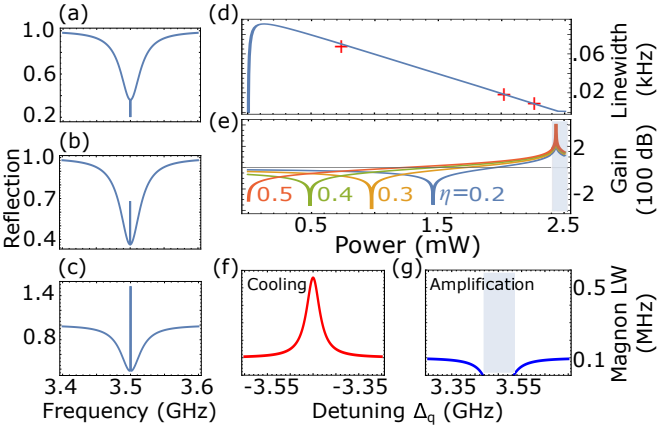

Figure 3. (a) to (e) Reflection of the lower side band probe with blue-detuned control at resonance with the magnon mode. (a) to (c) Reflection spectra for different control power (from top to bottom 0.78 mW, 2.01 mW and 2.26 mW, which have been labeled with "+" in (d)). The frequency (ω) is the sideband shift of the probe $\omega_{\rm p}$ from the control light ω_ℓ, $\omega = \omega_{\rm p} - \omega_\ell$. (d) The linewidth of the optomagnonic resonance as a function of the control power. (e) Gain at resonance as a function of the control power with varying $\eta = \kappa_{eq}/(2\kappa_q)$ for a given κ_q. The shaded area indicates the instable regime. (f) and (g) The linewidth of the magnon mode as a function of detuning for a given control power (11 mW). The red (blue) curve is obtained under the control light of red (blue) detuning. The shaded area indicates the parametric oscillation regime where the linewidth becomes negative. Parameters associated with the plots are $\kappa_q = 35$ MHz, $\gamma_m = 0.1$ MHz and $\Delta_q = -3.5$ GHz. η is fixed to be 0.2 in the figures other than (e). $\omega_k = 3.45$ GHz in (f) and (g).

damping rate moves the system from the undercoupled regime ($\eta = \kappa_{eq}/(2\kappa_q) < 0.25$) to the overcoupled one ($0.25 < \eta \leq 0.5$), and the critical power decreases so that the reflection becomes divergent more gradually, yielding more ability to control the effect experimentally [31].

To see the direction of power flow in the cavity, we plot the magnon linewidth as a function of detuning for a given control power in Figs. 3(f) and (g), considering the case with $\omega > 0$ only, which corresponds to Stokes (anti-Stokes) process for blue (red) detuning. Fig. 3 shows that for blue detuning the linewidth decreases as the detuning approaches the resonance with the magnon mode, which indicates that power flows from the control light to magnons, and that even parametric pumping of magnons can be achieved within the shaded range of the detuning. In contrast, for red detuning the linewidth increases as the detuning approaches the resonance with the magnon mode, which indicates that magnons can decay into the optical modes and thus the spin system can be cooled by detuning the control light. For a given γ_m and κ_q, increasing the control power (and thus $g^{\rm eff}$) will lead to the ultrastrong limit ($g^{\rm eff} > \gamma_m, \kappa_q$). We found that the corresponding magnon linewidth will not change qualitatively, but its magnitude will increase by orders of magnitude since it is proportional to $(g^{\rm eff})^2$.

To conclude, we have studied the photon-magnon interaction in an optical cavity made of a magnetic solid. The interaction is intrinsically greater than for optomechanics, and differs in character from the photon-magnon interaction in an microwave cavity. With control light and detuning of the probe light from the cavity resonance, this system can accomplish coherent conversion between a cavity mode and a magnon mode, or nonreciprocal conversion between two optical modes. As a basis for further studies of quantum dynamics, two classic coherent situations (electromagnetically induced transparency and the Purcell effect) have been simulated.

We acknowledge support of the Center for Emergent Materials, a NSF MRSEC under Award No. DMR-1420451 and DARPA MESO.

[1] A. H. Safavi-Naeini, T. P. M. Alegre, J. Chan, M. Eichenfield, M. Winger, Q. Lin, J. T. Hill, D. E. Chang, and O. Painter, Nature **472**, 69 (2011).
[2] T. P. Purdy, P.-L. Yu, R. W. Peterson, N. S. Kampel, and C. A. Regal, Phys. Rev. X **3**, 031012 (2013).
[3] K. Stannigel, P. Komar, S. J. M. Habraken, S. D. Bennett, M. D. Lukin, P. Zoller, and P. Rabl, Phys. Rev. Lett. **109**, 013603 (2012).
[4] H. Huebl, C. W. Zollitsch, J. Lotze, F. Hocke, M. Greifenstein, A. Marx, R. Gross, and S. T. B. Goennenwein, Phys. Rev. Lett. **111**, 127003 (2013).
[5] X. Zhang, C.-L. Zou, L. Jiang, and H. X. Tang, Phys.

Rev. Lett. **113**, 156401 (2014).
[6] Y. Tabuchi, S. Ishino, T. Ishikawa, R. Yamazaki, K. Usami, and Y. Nakamura, Phys. Rev. Lett. **113**, 083603 (2014).
[7] J. A. Haigh, N. J. Lambert, A. C. Doherty, and A. J. Ferguson, Phys. Rev. B **91**, 104410 (2015).
[8] L. Bai, M. Harder, Y. Chen, X. Fan, J. Xiao, and C.-M. Hu, Phys. Rev. Lett. **114**, 227201 (2015).
[9] J. A. Haigh, S. Langenfeld, N. J. Lambert, J. J. Baumberg, A. J. Ramsay, A. Nunnenkamp, and A. J. Ferguson, Phys. Rev. A **92**, 063845 (2015).
[10] X. Zhang, N. Zhu, C.-L. Zou, and H. X. Tang, arXiv:1510.03545 (2015).
[11] A. Osada, R. Hisatomi, A. Noguchi, Y. Tabuchi, R. Yamazaki, K. Usami, M. Sadgrove, R. Yalla, M. Nomura, and Y. Nakamura, arXiv:1510.01837 (2015).
[12] J. Bourhill, N. Kostylev, M. Goryachev, D. Creedon, and M. Tobar, arXiv:1512.07773 (2015).
[13] S. Gröblacher, K. Hammerer, M. R. Vanner, and M. Aspelmeyer, Nature **460**, 724 (2009).
[14] J. T. Hill, A. H. Safavi-Naeini, J. Chan, and O. Painter, Nat Commun **3**, 1196 (2012).
[15] S. Kolkowitz, A. C. B. Jayich, Q. P. Unterreithmeier, S. D. Bennett, P. Rabl, J. G. E. Harris, and M. D. Lukin, Science **335**, 1603 (2012).
[16] C. Dong, V. Fiore, M. C. Kuzyk, and H. Wang, Science **338**, 1609 (2012).
[17] B. Gouraud, D. Maxein, A. Nicolas, O. Morin, and J. Laurat, Phys. Rev. Lett. **114**, 180503 (2015).
[18] E. M. Purcell, Phys. Rev. **69**, 681 (1946).
[19] C.-H. Su, A. D. Greentree, and L. C. L. Hollenberg, Optics Express **16**, 6240 (2008).
[20] L. Li, T. Schröder, E. H. Chen, M. Walsh, I. Bayn, J. Goldstein, O. Gaathon, M. E. Trusheim, M. Lu, J. Mower, M. Cotlet, M. L. Markham, D. J. Twitchen, and D. Englund, Nat Commun **6**, 6173 (2015).
[21] W. Wettling, M. G. Cottam, and J. R. Sandercock, Journal of Physics C: Solid State Physics **8**, 211 (1975).
[22] W. Wettling, Applied physics **6**, 367 (1975).
[23] T. Holstein and H. Primakoff, Phys. Rev. **58**, 1098 (1940).
[24] D. D. Stancil, IEEE Journal of Quantum Electronics **27**, 61 (1991).
[25] The optical cavity in the three systems is taken to be the same, with $l \times w \times d = 8\,\mathrm{mm} \times 400\,\mu\mathrm{m} \times 4\,\mu\mathrm{m}$. For the electro-optical system, we use the parameters of lithium niobate, with $n_0 = 2.3$, $r = 308\,\mathrm{pm/V}$, $\omega_m = 2\pi \times 9\,\mathrm{GHz}$, and $C = 1\,\mathrm{pF}$. For the optomechanical system, $m = 145\,\mathrm{ng}$, and $\omega_m = 2\pi \times 947\,\mathrm{kHz}$. For the optomagnonic system (made of YIG), $K = 4.76 \times 10^{-9}\,\mathrm{m/A}$, $n_0 = 2.2$, and $M_0 = 1.39 \times 10^5\,\mathrm{A/m}$.
[26] M. Tsang, Phys. Rev. A **81**, 063837 (2010).
[27] N. Brahms and D. M. Stamper-Kurn, Phys. Rev. A **82**, 041804 (2010).
[28] G. E. Marti, A. MacRae, R. Olf, S. Lourette, F. Fang, and D. M. Stamper-Kurn, Phys. Rev. Lett. **113**, 155302 (2014).
[29] F. Fang, R. Olf, S. Wu, H. Kadau, and D. M. Stamper-Kurn, Phys. Rev. Lett. **116**, 095301 (2016).
[30] P. Siddons, C. S. Adams, C. Ge, and I. G. Hughes, J. Phys. B: At. Mol. Opt. Phys. **41**, 155004 (2008).
[31] X. Zhang, C.-L. Zou, L. Jiang, and H. X. Tang, Science Advances **2**, e1501286 (2016).